

KLLM: Fast LLM Inference with K-Means Quantization

Xueying Wu, Baijun Zhou, Zhihui Gao, Yuzhe Fu, Qilin Zheng, Yintao He[†], and Hai “Helen” Li

Department of Electrical and Computer Engineering, Duke University

Email: {xueying.wu, baijun.zhou, zhihui.gao, yuzhe.fu, qilin.zheng, yintao.he, hai.li}@duke.edu

Abstract—Large language model (LLM) inference poses significant challenges due to its intensive memory and computation demands. Weight and activation quantization (WAQ) offers a promising solution by reducing both memory footprint and arithmetic complexity. Traditional WAQ designs rely on *uniform* integer quantization for hardware efficiency, but often suffer from significant model performance degradation at low precision. In contrast, K-Means quantization, a *non-uniform* technique, achieves higher accuracy by aligning with the Gaussian-like distributions of weights and activations in LLMs. However, two key challenges prevent the efficient deployment of K-Means-based WAQ designs for LLM inference: (1) The non-uniform structure of K-Means-quantized data precludes direct execution on low-precision compute units, necessitating dequantization and floating-point matrix multiplications (MatMuls) during inference. (2) Activation outliers hinder effective low-precision quantization. Offline thresholding methods for outlier detection degrade model performance substantially, while existing online detection techniques introduce significant runtime overhead.

To address the aforementioned challenges and fully unleash the potential of K-Means-based WAQ for LLM inference, in this paper, we propose KLLM, an LLM inference accelerator for efficient execution with K-Means-quantized weights and activations. KLLM features an index-based computation scheme for efficient execution of MatMuls and nonlinear operations on K-Means-quantized data, which avoids most of the dequantization and full-precision computations. Moreover, KLLM incorporates a lightweight outlier detection engine, *Orizuru*, that efficiently identifies the top- k largest and smallest elements in the activation data stream during online inference.

Extensive experiments show that, KLLM achieves speedups of $8.66\times$, $2.12\times$ and energy efficiency improvements of $214.76\times$, $2.79\times$ compared to the A100 GPU and SpAtten, respectively.

I. INTRODUCTION

Large language models (LLMs) have achieved impressive advancements, demonstrating versatile applications such as chatbots [1], [18], code generation [41], [46], and circuit design [14], [20]. However, the enormous sizes of LLMs pose significant challenges for inference, demanding substantial memory [5], [27] and computational resources [7], [12].

Matrix multiplications (MatMuls) dominate the execution time of LLM inference [58]. To address this bottleneck, weight and activation quantization (WAQ) methods have been proposed to enable low-precision MatMuls, which reduce both memory usage and computational costs [3], [55], [61]. Existing WAQ methods primarily leverage integer quantization, which represents data with equally spaced quantization centroids [23], [55]. However, this uniform spacing fails to align with the actual distributions of LLM weights and activations, which often exhibit non-uniform Gaussian-like patterns,

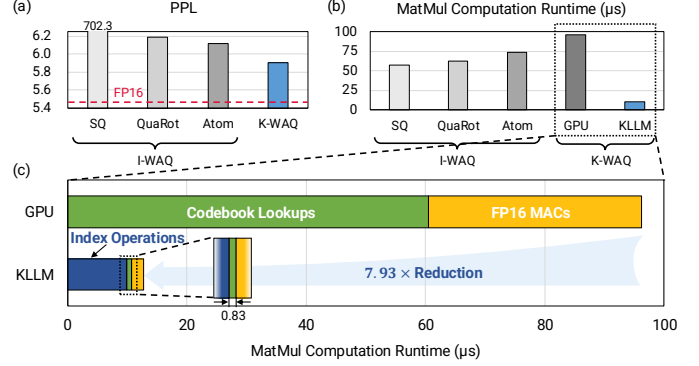


Fig. 1. (a) PPL comparison across W4A4 I-WAQ and K-WAQ methods. (b) MatMul runtime and (c) runtime breakdown of W4A4 kernels on A100 GPU vs. KLLM accelerator. Runtime in both (b) and (c) are measured for a MatMul between a 4096×4096 weight matrix and a 1×4096 activation vector.

with most values concentrated around the mean [22], [25]. Therefore, integer WAQ (I-WAQ) methods often suffer from high quantization noises and significant degradation in model performance, especially at low quantization precisions. For example, as shown in Figure 1(a), the W4A4 perplexity (PPL) of LLaMA-2-7B [48] on WikiText-2 [34] with SmoothQuant [55] is 702.3, which is $127\times$ higher than the FP16 model. To mitigate PPL degradation, recent I-WAQ methods such as QuaRot [3] and Atom [61] employ techniques of Hadamard transformations and group-wise quantization to reduce quantization noise. Unfortunately, as shown in Figure 1(a), these techniques still result in noticeable PPL degradation compared to FP16 models. Moreover, as shown in Figure 1(b), these techniques also lead to increased runtime overhead, which is caused by additional matrix operations and reduced computational parallelism of MatMuls. Overall, existing I-WAQ methods exhibit noticeable model performance degradation and high runtime overhead, despite leveraging integer compute units.

Compared to uniform integer quantization, the non-uniform quantization method of K-Means clustering [33] could better align with data distributions and reduces quantization noises. This is because K-Means determines quantization centroids through an optimization process that allocates more centroids to regions with higher data density. This non-uniform allocation improves data representation fidelity, especially in low-precision configurations [22], [25]. However, the non-uniform nature of K-Means-quantized data makes it incompatible with integer compute units. Consequently, data must be dequantized back to FP16 format, and MatMuls are performed on FP16

[†]Yintao He is the corresponding author of this paper.

compute units. As illustrated in Figure 1 (b), this leads to even higher runtime for K-Means WAQ (K-WAQ) compared to I-WAQ methods when implemented on an NVIDIA A100 GPU [36]. Figure 1 (c) further reveals that codebook lookups during dequantization dominate the MatMul runtime, accounting for 63% of the total execution time. Thus, to fully unleash the potential of K-WAQ for LLM inference acceleration, it is crucial to design an efficient computation scheme and customized compute units capable of directly processing the integer indices of K-Means-quantized data, eliminating the need for dequantization.

To address the aforementioned challenges, in this work, we propose KLLM, an LLM inference accelerator for efficient execution with K-Means-quantized weights and activations. KLLM introduces an index-based computation scheme, along with customized low-precision compute units that directly process the integer indices of K-Means-quantized data. As illustrated in Figure 1 (c), during MatMul computation, KLLM significantly reduces the runtime of codebook lookups and FP16 multiply-accumulates (MACs), while introducing minimal overhead for index-based operations. KLLM achieves a $7.93\times$ speedup for a W4A4 MatMul with K-WAQ compared to the A100 GPU. This computation scheme also provides significant speedup for nonlinear operations in LLMs. Moreover, we design an efficient top- k largest and smallest element detection engine named *Orizuru* for dynamically identifying activation outliers, which effectively mitigates quantization errors.

We compare KLLM with state-of-the-art quantization algorithms and accelerators. For the algorithmic performance, KLLM achieves a PPL of 5.90 for LLaMA-2-7B [48] model on WikiText-2 [34] dataset with W4A4 K-WAQ, which corresponds to a PPL degradation of 0.43 compared to the FP16 model. This PPL degradation is 34% lower than that of Atom [61]. For the hardware performance, KLLM under W4A4 configuration achieves average speedups of $8.66\times$, $2.12\times$ and energy efficiency improvements of $214.76\times$, $2.79\times$ compared to the A100 GPU and SpAtten [49], respectively.

The main contributions of this work are summarized as:

- We propose an efficient index-based computation scheme that supports both MatMul and nonlinear operations for LLMs with K-Means-quantized data.
- We design KLLM, an LLM inference accelerator that executes the proposed index-based scheme on customized low-precision compute units with high efficiency.
- We propose *Orizuru*, an efficient top- k largest and smallest element detection engine for dynamic outlier identification.

II. MOTIVATION

As discussed in §I, I-WAQ designs face significant limitations in low-precision LLM quantization, which include: (1) noticeable PPL degradation compared to FP16 models, and (2) substantial runtime overhead despite utilizing low-precision compute units. To achieve higher model performance in low-precision LLM inference, K-WAQ methods are required. However, we identify two key challenges in accelerating LLM inference with K-WAQ, as discussed below.

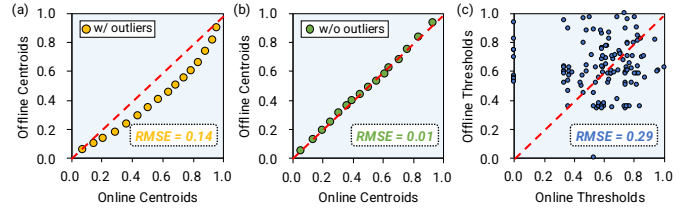


Fig. 2. Comparison of 4-bit K-Means quantization centroids for activations trained (a) with and (b) without outliers across online and offline datasets. (c) Normalized upper thresholds of activation outliers computed on the online and offline datasets. The activations used to compute the centroids and thresholds are the input of the first q_{proj} layer in the LLaMA-2-7B model. 128 activation tokens are applied, each with the dimension of 1×4096 . The online and offline datasets are WikiText-2 [34] and C4 [11], respectively.

A. Challenges

1) *Inefficiencies of Executing MatMuls with K-Means-Quantized Data:* Although K-WAQ exhibits superior model performance at low precision, it incurs inefficient MatMuls execution during inference, resulting in higher runtime than traditional I-WAQ methods in Fig. 1(b). This is because K-Means quantization produces non-uniform quantized data, which cannot be directly processed by integer compute units. In K-Means quantization, each matrix is represented by an integer index matrix and a floating-point centroid codebook. Each integer index points to a corresponding centroid in the codebook [33], which serves as an approximate reconstruction of the original value. To perform MatMuls, the integer index matrices must be dequantized into floating-point representations. To be specific, consider $Y_{1 \times N} = A_{1 \times K} \cdot B_{K \times N}$, which is the common case for single-batch decoding during LLM inference. $\tilde{A}_{1 \times K}$ and $\tilde{B}_{K \times N}$ represent the integer index matrices for A and B , respectively, while C_A and C_B denote their corresponding centroid codebooks. s_A and s_B are the scaling factors, and z_A and z_B are the zero points. The MatMul operation can be formulated as:

$$Y_n = \sum_{k=1}^K \underbrace{s_A (C_A[\tilde{A}_k] - z_{A_k})}_{A_k} \cdot \underbrace{s_{B,n} (C_B[\tilde{B}_{k,n}] - z_{B,n})}_{B_{k,n}}. \quad (1)$$

Since C_A and C_B are floating-point values, the MatMul operation should be executed on floating-point compute units instead of the efficient integer compute units. Therefore, dequantization for the integer index matrices \tilde{A} and \tilde{B} is required, which involves per-element codebook lookups. Both dequantization and the subsequent floating-point MatMul computation introduce substantial runtime overhead. Therefore, it is crucial to develop an efficient index-based computation scheme that can directly process the index matrices of \tilde{A} and \tilde{B} . Additionally, customized compute units that can efficiently execute this scheme are also required.

2) *Activation Outlier Thresholding:* To utilize efficient low-precision compute units during LLM inference, both weights and activations should be quantized. While weight quantization

can be performed offline with pre-trained centroids, it is impractical to conduct the time-consuming K-Means centroid training for dynamic activations during online inference. To address this, we adopt offline-calculated centroids to quantize the activations during online inference, an approach proposed in [22] for KV Cache quantization. This approach computes the K-Means centroids using an offline calibration dataset without runtime training overhead. However, applying this approach to quantize the full set of LLM activations leads to significant model performance degradation. This is caused by the discrepancies between the centroids computed with online and offline datasets, as shown in Figure 2 (a).

On the other hand, we observe that excluding activation outliers from quantization significantly improves the consistency of online and offline centroids, as illustrated in Figure 2 (b). Outliers, which are the extreme values deviating from the majority of the data, can cause significant distortion on quantization centroids [61]. In Figure 2 (b), the top 0.5% largest and smallest activation values are excluded from quantization in both online and offline datasets. This reduces the root mean square error (RMSE) between the online and offline centroids of the two datasets from 0.14 to 0.01, significantly improving their alignment. Therefore, to maintain model performance, it is essential to detect and exclude outliers from quantization.

To identify activation outliers during online inference, prior studies have utilized offline-calculated thresholds derived from a calibration dataset [2], [61]. However, as shown in Figure 2 (c), the outlier threshold distributions of online and offline activations differ significantly, with an RMSE of 0.29. Since the scaling factors, which are determined by the outlier thresholds, have a critical impact on quantization errors, this discrepancy leads to noticeable model performance degradation, as demonstrated in §V-B. To address this issue and ensure that the quantization thresholds are consistent with the current input data, it is essential to dynamically detect activation outliers during online inference.

B. Our Approach

We aim to achieve efficient LLM inference with high model performance by leveraging K-WAQ. To address the challenges discussed in §II-A, we propose KLLM, a hardware-software co-design framework. Specifically, we focus on the following two aspects: (1) introducing an efficient index-based computation scheme for K-Means-quantized data and corresponding customized compute units that can efficiently execute this scheme, and (2) developing a lightweight outlier detection engine that dynamically identifies top- k activation values during online inference.

III. ALGORITHMIC OPTIMIZATIONS

§III-A presents the K-Means-based quantization method used in KLLM, which encodes both weights and activations into integer index matrices and floating-point centroid codebooks. Building on this data representation, §III-B introduces our proposed index-based computation scheme, which directly

performs MatMul operations using the quantized data, avoiding most of the time-consuming dequantization and floating-point operations. We further extend this scheme in §III-C to support nonlinear operations in LLMs, enabling end-to-end efficient index-based computations in LLM inference. For simplicity, scaling factors and outliers are omitted in §III-B. The complete computation flow for MatMuls, including scaling factors and outliers, is detailed in §III-D.

A. Quantizing Weights and Activations

KLLM performs K-Means quantization on both weights and activations in the LLMs. Specifically, we employ output-channel-wise quantization for weights and token-wise quantization for activations. To further mitigate model performance degradation caused by activation quantization, we preserve $\sim 1\%$ of the activation outliers in floating-point format. KLLM aims to optimize the computations of both MatMul and nonlinear operations with the index-based computation scheme. Therefore, all activations in the LLMs are quantized using K-Means quantization, with only two exceptions of attention weights and attention scores, which are the input and output of the SoftMax function, respectively. The attention weights are preserved in FP16 format, as SoftMax is highly input-sensitive [56]. On the other hand, we apply integer quantization on the attention scores. This is based on the observations that (1) quantizing attention scores with integer and K-Means quantization yields similar PPL, and (2) the index-based MatMul scheme is more efficient when one multiplicand uses K-Means quantization and the other uses integer quantization, rather than when both use K-Means, as shown in §III-B2.

B. Index-Based Computation for MatMuls

As discussed in §II-A1, to execute MatMul operations with K-Means quantized data, time-consuming dequantization and floating-point operations are required. To address this, we propose an index-based computation scheme that eliminates the need for dequantization by directly operating on quantized representations. Specifically, we observe that when both operands of the MatMuls are quantized, the set of possible products becomes finite and fixed. These products can be precomputed offline using the centroids of weights and activations. During inference, MatMul is reformulated as a weighted sum over these precomputed products. The weights for the weighted sum are derived from the distribution of indices and computed using lightweight integer operations. This design shifts most of the computational workload to offline preprocessing, enabling online inference with minimal floating-point cost. Next, we first walk through an example of the index-based computation scheme, where both multiplicands are K-Means-quantized, as shown in Figure 3(a). Then, we introduce optimizations for the case where one multiplicand is K-Means-quantized and the other is integer-quantized, as illustrated in Figure 3(b).

1) *K-Means-K-Means MatMuls*: Consider the example $Y_{1 \times N} = A_{1 \times K} \cdot B_{K \times N}$, where n_A and n_B are the precisions of A and B , respectively. To be specific, consider the example

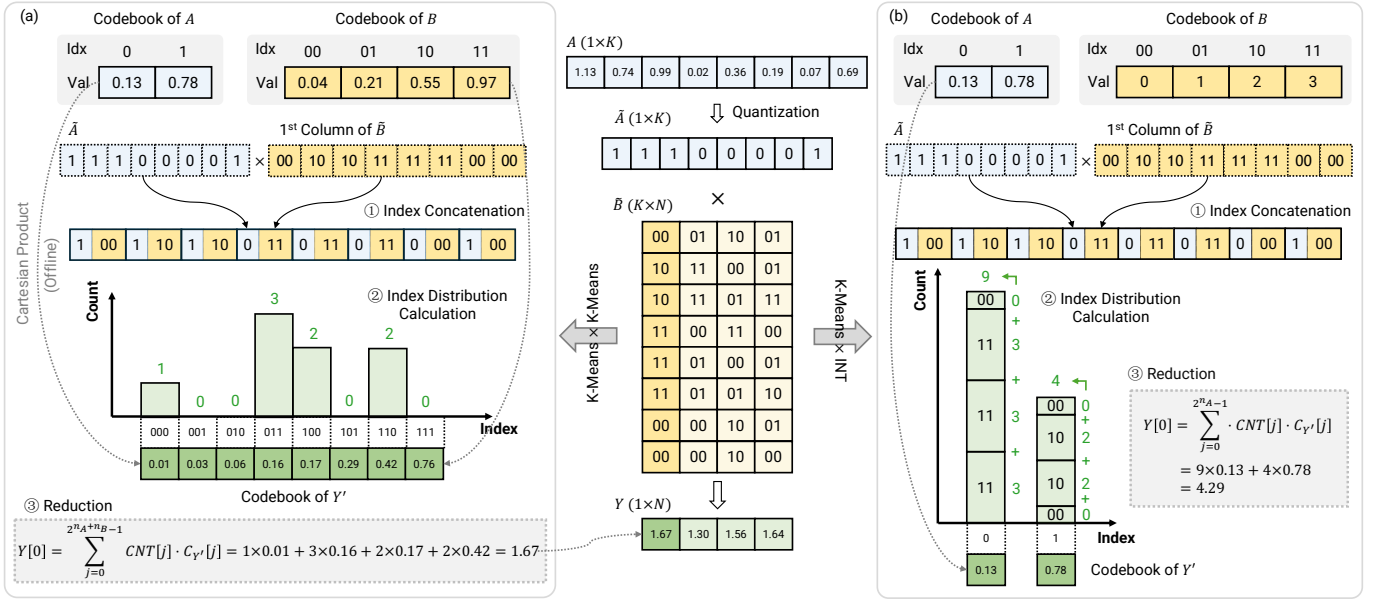


Fig. 3. Index-based MatMul scheme where (a) both multiplicands are K-Means-quantized data (b) one multiplicand is integer-quantized and the other is K-Means-quantized.

$Y_{1 \times N} = A_{1 \times K} \cdot B_{K \times N}$, where n_A and n_B are the precisions of A and B , respectively. In Figure 3, $N = 4, K = 8, n_A = 1$, and $n_B = 2$. Let $Y' = [A^T \odot B_1, \dots, A^T \odot B_N] \in \mathbb{R}^{K \times N}$ be the product of the element-wise multiplication, where $B_i \in \mathbb{R}^{K \times 1}$ is the i -th column of B , \odot denotes element-wise multiplication, and $Y = [\sum_i Y'_{i,1}, \dots, \sum_i Y'_{i,N}]$. We note that Y' contains only $2^{n_A+n_B}$ values. Therefore, the Cartesian products of the quantization centroids of A and B , which only require $2^{n_A+n_B}$ multiplications, are sufficient to compute the distinct values in Y' . Moreover, since the quantization centroids of A and B are pre-calculated offline, the Cartesian products can also be conducted offline. Computing the reduction of the partial sum matrix Y' requires 3 steps. In step ①, to get the indices of the partial sum matrix Y' , we perform element-wise index concatenation of vector A with each column of matrix B . The resulting index matrix \tilde{Y}' has a precision of $n_A + n_B$. Step ② calculates the distribution of the indices in each column of \tilde{Y}' . Once the distribution is obtained, in step ③, we compute the weighted sum of the $2^{n_A+n_B}$ distinct values in each column of Y' . In this way, to compute the MatMul with each column of B , the number of online MACs required is reduced from K to $2^{n_A+n_B}$, which is significantly smaller in low-precision quantization scenarios. For example, in W4A4 configurations, where n_A and n_B are both 4, $2^{n_A+n_B} = 256$ is much smaller than $K = 4096$, which is a common dimension in LLMs [12]. Note that the index-based MatMul scheme can support arbitrary precisions for both multiplicands, and does not require the precision of the two multiplicands to be equal.

2) *Integer-K-Means MatMuls*: The index-based MatMul computation is able to achieve higher efficiency when one multiplicand is K-Means-quantized and the other is integer-quantized. Integer quantization can be considered a special

case of K-Means quantization, where the quantization centroids and the indices are the same. Therefore, the element-wise multiplications between the K-Means and integer centroids can be viewed as integer multiples of the K-Means centroids. In Figure 3(b), without loss of generality, assume A is K-Means-quantized while B is integer-quantized. Instead of calculating the Cartesian product of the centroids of A and B , we directly use the codebook of A as the codebook of Y' . As shown in step ② of Figure 3(b), to calculate the index distribution in each column of Y' , the count of the corresponding index of \tilde{Y}' increments by the value of the corresponding index of B , rather than “+1” as in the case of K-Means-K-Means MatMul. This optimization significantly reduces the runtime of index distribution counting, as the number of distinct indices in Y' is reduced from $2^{n_A+n_B}$ to 2^{n_A} . It also further reduces the number of MACs required for the MatMul with each column of B from $2^{n_A+n_B}$ to 2^{n_A} .

C. Index-Based Nonlinear Operations

Nonlinear operations, such as activation and normalization functions, can introduce significant runtime during LLM inference due to their complexity and limited on-chip resources [10], [51]. Fortunately, the index-based computation scheme can also accelerate the nonlinear operations given that the activations are quantized.

1) *Activation Function*: Activation functions in LLMs, such as SiLU [13] and GELU [21], are element-wise operations, i.e., each output value of the activation function depends only on a single input scalar. Assuming that the input of the activation function is n -bit quantized, the number of distinct values in the input activation is 2^n . Consequently, the output of the activation function will also have only 2^n distinct values, with the input and output sharing identical index vectors. Since the

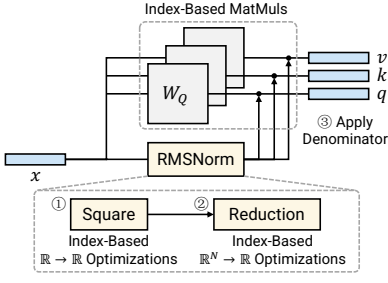


Fig. 4. Computation optimizations for RMSNorm.

quantization centroids of the input are pre-calculated offline, we can also pre-compute the activation function’s outputs for these centroids offline, which then become the centroids for the output activation. During online inference, we simply replace the centroids in the codebook of the input activation with the corresponding centroids for the output activation, keeping the activation’s index vector unchanged. This achieves an efficient computation of the activation function with minimal runtime latency. Note that besides activation functions, this optimization can also be applied to all $\mathbb{R} \rightarrow \mathbb{R}$ functions.

2) *Normalization Function*: In most LLMs, the inputs to both the MHA and FFN modules are normalized using either RMSNorm [60] or LayerNorm [4]. Consider RMSNorm, as defined in Equation 2. Its computation involves three steps: ① element-wise squaring of the input vector, ② a reduction operation to compute the mean of the squared values, and ③ dividing the input elements by the square root of the mean.

$$\text{RMSNorm}(x) = \frac{x}{\text{RMS}(x)} = \frac{x}{\sqrt{\frac{1}{N} \sum_{i=1}^N x_i^2}}. \quad (2)$$

As illustrated in Figure 4, KLLM *parallelizes* the RMSNorm computations with the subsequent index-based MatMuls based on the observation that the MatMuls are linear functions, and *delaying the division by the denominator* of RMSNorm does not affect the correctness of the computation. Furthermore, KLLM provides significant acceleration for all three steps of the RMSNorm function: the number of square operations in step ① is reduced from N to 2^n , as these are $\mathbb{R} \rightarrow \mathbb{R}$ functions, which can be optimized using the index-based approach described in §III-C1; the reduction operation in step ②, being an $\mathbb{R}^N \rightarrow \mathbb{R}$ function, is simplified into weighted sums requiring only 2^n FP MACs, leveraging the same optimization as the reduction step in index-based MatMuls; and in step ③, the division is fused into the scaling factors of the MatMul operations. Specifically, the denominator of the RMSNorm function is incorporated into the input activation’s scaling factor (a scalar) and the weight matrix’s centroids (2^{n_W} scalars, where n_W is the precision of weight), significantly reducing the number of FP divisions required. Similar optimizations can be extended to LayerNorm: the mean and standard deviation computations required for LayerNorm can be performed in a manner analogous to RMS.

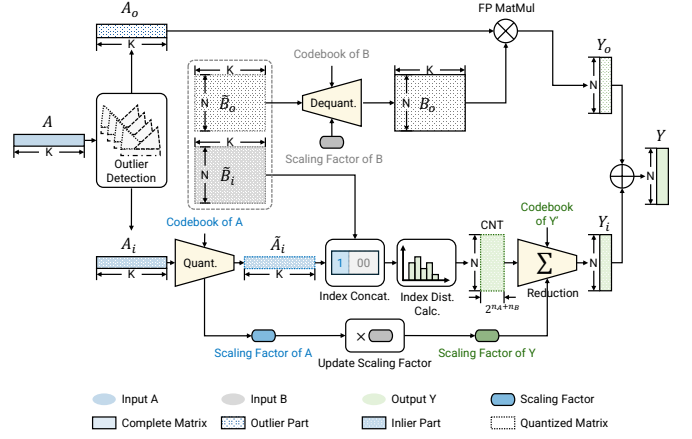


Fig. 5. Comprehensive index-based MatMul computation flow.

D. Overall Computation Flow

Figure 5 shows the comprehensive computation flow for a MatMul operation $A_{1 \times K} \cdot B_{K \times N} = Y_{1 \times N}$ using the index-based computation scheme, incorporating scaling factors and outliers. Starting with an FP16 input activation vector A , the *Orizuru* units generate an outlier mask that divides A into a sparse outlier component A_o and a dense inlier component A_i . The quantized weight matrix \tilde{B} is also partitioned into a dense portion \tilde{B}_i and a sparse portion \tilde{B}_o according to the outlier mask. \tilde{B}_i is multiplied with the quantized inlier activation \tilde{A}_i using the index-based MatMul scheme described in §III-B. During this process, the scaling factor of A is multiplied by that of \tilde{B} to form the scaling factor of Y , which is applied to the intermediate result Y_i during reduction. Simultaneously, the sparse matrix \tilde{B}_o is dequantized to FP16 format as B_o and multiplied with A_o using sparse FP16 MatMuls. Finally, the partial results Y_i and Y_o from the dense and sparse paths are summed to produce the output vector Y .

IV. KLLM ACCELERATOR

To enable the efficient execution of the index-based computation scheme introduced in §III, in this section, we present the supporting accelerator design of KLLM. Moreover, KLLM accelerator also features a lightweight outlier detection engine, *Orizuru*, which is designed to efficiently identify the top- k largest and smallest elements in each activation token.

A. Overall Architecture

Figure 6 shows the overall architecture of the KLLM accelerator, and Table I presents the hardware configurations. The KLLM accelerator is composed of 16 Processing Element (PE) Lanes, an Activation Buffer storing the index and codebook, an Output Buffer storing the output values and an outlier mask, Clustering Units for K-Means clustering, *Orizuru* units that generate the outlier mask, and a Functional Unit to handle complex operations such as square roots and exponentials. Each PE Lane contains a Weight Buffer, 4096 Concat units, 32 16-input Index Distribution Counters, and

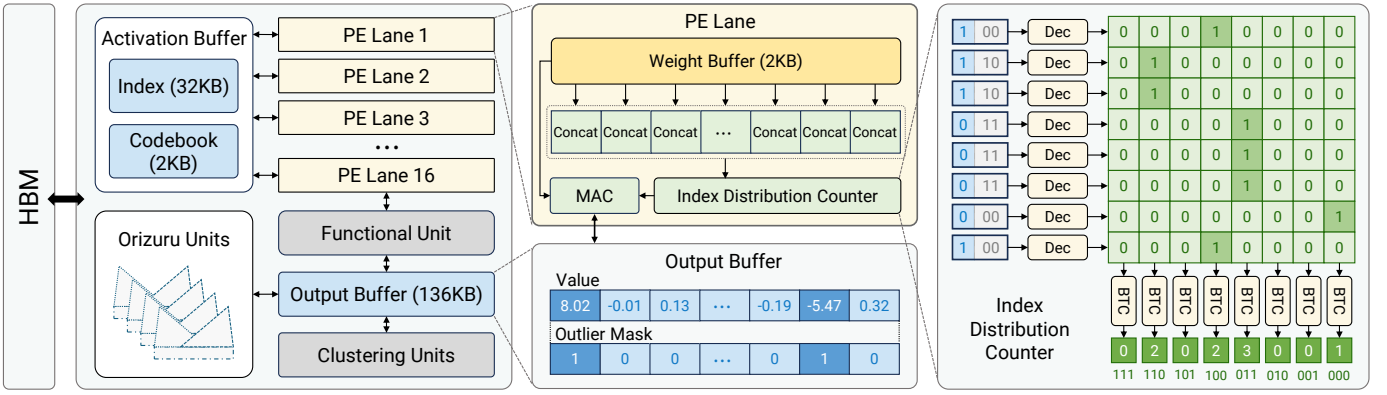


Fig. 6. Overall architecture of the KLLM accelerator.

32 FP16 MAC units. A Concat unit concatenates two 4-bit inputs and stores the result in an 8-bit register. Due to its simple design, the Concat unit provides significantly higher area efficiency than the FP16 MAC units, allowing for a total of 65,536 Concat units on the chip. The FP16 MAC units handle the weighted-sum operations in the reduction step, sparse FP16 multiplications between activation outliers and the weights, the FP16 additions that combine the partial results of sparse multiplications with dense multiplications, as well as activation clustering. Activation Index Buffer stores the activation indices. For Integer-K-Means MatMuls, the Act Codebook Buffer stores the codebook of the activation centroids, while for the K-Means-K-Means MatMul, it stores the offline-calculated Cartesian product of the two codebooks. The hardware design of the Index Distribution Counter and the *Orizuru* unit is discussed in §IV-B and §IV-C, respectively.

In KLLM, all activations except the attention weights are quantized, and the computation complexities involving the quantized activations are significantly decreased. Thus, SoftMax, which takes the unquantized attention weights as input, becomes the bottleneck during LLM inference. However, we observe that the MatMuls for the attention scores and V are independent across different attention heads. Therefore, the SoftMax operation for the $i + 1$ -th head of the attention weights can be conducted concurrently with the MatMuls for the i -th head of the attention scores and V . There are 8 exponential units in the Functional Unit, parallelizing the SoftMax operations. This enables the efficient attention-head-wise pipeline execution of SoftMax and the subsequent MatMul.

B. Index Distribution Counter

The Index Distribution Counter is designed to efficiently compute the index distribution of the partial-sum matrix C' , as depicted on the right side of Figure 6. In the K-Means-K-Means MatMul scenario, given K concatenated indices, the Index Distribution Counter decodes these indices into one-hot vectors in parallel, forming a matrix of size $K \times 2^{n_A + n_B}$, where K is the reduction dimension, and n_A and n_B represent the precisions of the two input matrices. Subsequently, the bit counters (BTCs) in the Index Distribution Counter calculate

TABLE I
KLLM ACCELERATOR CONFIGURATIONS (28NM, 500MHz).

Module	Specification	Area (mm^2)	Power (W)
PE Lane	16 PE Lanes per chip	8.25	5.73
PE Lane	Concat Unit	$4096 \text{ Concat Units per lane}$	8.68×10^{-2}
	Wgt Buffer	2 KB per lane	6.75×10^{-2}
	IdxCounter	$32 \text{ 16-in IdxCounter per lane}$	2.71×10^{-1}
	MAC	$32 \text{ FP16 MAC Units per lane}$	9.05×10^{-2}
Out Buffer	136 KB per chip	4.61	5.70×10^{-1}
Act Idx Buffer	32 KB per chip	2.16	5.40×10^{-1}
Act Codebook Buffer	2 KB per chip	8.44×10^{-3}	2.11×10^{-3}
Clustering Unit	1 Clustering Unit per chip	2.11×10^{-1}	7.10×10^{-1}
Orizuru	273 16-in Orizuru Units per chip	7.39×10^{-1}	2.73×10^{-1}
Functional Unit	1 Functional Unit per chip	8.89×10^{-1}	5.63×10^{-1}
Total	—	16.87	8.96

the column-wise sums of the $K \times 2^{n_A + n_B}$ matrix, which correspond to the frequency of each index in the concatenated indices. In the Integer-K-Means MatMul scenario, only the indices of matrix A are decoded into one-hot vectors, and the BTCs compute the weighted-sums of the $K \times 2^{n_A}$ matrix in each column, with the weights being the corresponding values in matrix B . To satisfy timing and area constraints, the Index Distribution Counter employs a 16-input design, with each PE Lane incorporating 32 Index Distribution Counters to perform the index distribution calculations in parallel.

C. Orizuru: Dynamic Outlier Detection Engine

As mentioned in §III-A, we propose to detect 1% of the outliers within each activation token $\mathbf{x} = [x_i] \in \mathbb{R}^N$, which are excluded from the quantization process. Specifically, the 0.5% largest and the 0.5% smallest activations are preserved. To enable efficient online identification of the outliers for KLLM, we propose an efficient outlier detection engine named *Orizuru*¹ that picks the k maximums and k minimums from an N -input activation vector \mathbf{x} at the cost of $1.5N + 2k \cdot \log_2(N)$ comparisons. As shown in Fig. 7(a), the proposed *Orizuru* is composed of two complete binary trees with shared leaf

¹The shape of the two-fold binary trees with shared leaves resembles an *Orizuru* (a paper crane).

nodes. These two binary trees, named the max tree, \mathcal{P} , and the min tree, \mathcal{Q} , are used to pop the k largest and smallest elements of a given vector \mathbf{x} , respectively. The tree structure offers high data reuse for input data, reducing memory access overhead. Without loss of generality, we take the max tree as an illustration of how we initialize, pop out, and maintain the tree; then we showcase how we reuse the information from the max tree to the min tree towards the *Orizuru* architecture.

Complete binary tree architecture For simplicity, in the example of Figure 7, we consider an 8-input *Orizuru* for $N = 8$. Specifically for the max tree, \mathcal{P} , as shown in Figure 7(b), we build a complete binary tree with L levels, where $L = \log_2(N)$. Each node on the tree is a 2-to-1 multiplexer (MUX) controlled by the value in a bit buffer, denoted as $p_{l,i} \in [0, 1]$, where $l = 1, 2, \dots, L$ is the level index and $i = 1, 2, \dots, 2^{l-1}$ is the node index of this level. For the $N/2$ leaf nodes on the L -th level, the node $p_{L,i}$ is directly connected to the FP16 values of x_{2i-1} and x_{2i} ; the non-leaf node $p_{l,i}$ is connected to its left/right children $p_{l+1,2i-1}$ and $p_{l+1,2i}$, and its MUX outputs

$$\text{MUX}(p_{l,i}) = \begin{cases} \text{MUX}(p_{l+1,2i-1}) \text{ or } x_{2i-1}, & p_{l,i} = 0 \\ \text{MUX}(p_{l+1,2i}) \text{ or } x_{2i}, & p_{l,i} = 1. \end{cases} \quad (3)$$

In the max tree, \mathcal{P} , the bit buffer points to the larger child node or activation value, which represents the largest element in the sub-tree rooted at the current node. Consequently, the output of the root node, $\text{MUX}(1, 1)$, corresponds to the largest value in the entire activation vector, $\max(\mathbf{x})$. To track the availability of activation elements, we introduce a mask vector $\mathbf{m}^{(p)} = [m_i^{(p)}] \in [0, 1]^N$ for the max tree \mathcal{P} , where $m_i^{(p)} = 1$ indicates that the activation element x_i is available, and $m_i^{(p)} = 0$ indicates it has already been popped out. Similarly, another independent mask vector $\mathbf{m}^{(q)} = [m_i^{(q)}] \in [0, 1]^N$ is defined for the min tree \mathcal{Q} .

Initializing the binary tree To initialize the max and min trees for a new activation vector \mathbf{x} , we update all the bit buffers tree. This process is performed in a bottom-up manner across the L levels of the tree. Initially, at the $\log_2(N)$ -th level, the registers of the non-leaf nodes (e.g., nodes 4, 5, 6, and 7) are updated by comparing their left and right child nodes at the leaf level, which hold the input values. This step involves $N/2$ comparisons. After completing these comparisons, the registers are updated to indicate whether the left or right child contains the larger value. Next, this comparison process is repeated recursively for each level, moving upwards until the root node's register is updated. Finally, the MUX at the root node selects the maximum value from the N elements. Overall, the tree initialization requires $N - 1$ FP16 comparisons.

Popping up and maintaining the tree Once the initialization is complete, the maximum value can be popped out immediately. The index of this maximum value is determined by traversing the tree from the root node to the corresponding leaf node, following the binary digits stored in the registers. For example, to locate the index of the maximum element “9”

(at node 14) in Figure 7(b), we start at the root node, which contains “1”, directing us to its right child, node 3. Node 3 also contains “1”, further directing us to its right child, node 7. This process continues for $\log_2(N)$ steps until we reach the maximum element “9” at node 14. The binary digits from the accessed registers are concatenated to form “110”. Since leaf nodes are indexed from N to $2N - 1$, a “1” is prefixed to the concatenated value, resulting in “1110”—the binary representation of the index “14” for the maximum value “9”. Note that this process does not involve any comparisons and can be completed in one clock cycle.

To identify the second largest value, the popped maximum value must first be effectively “removed” from the tree, which is the tree maintenance process. This is achieved by updating the registers of the non-leaf nodes while maintaining the tree structure. As shown in Figure 7(c), the updated information is highlighted with red Max val indicators and arrows. Specifically, the popped maximum value is treated as negative infinity during the update for the register value of its parent node while the original value remains unchanged in the FP16 buffer of the corresponding leaf node. Consequently, the arrow in the parent node flips to point to the neighbor node of the popped value.

The registers on the ancestors of the popped element are updated in a bottom-up manner. This maintenance process resembles the initialization but involves only a single comparison per level. Each maintenance step requires $\log_2(N)$ sequential comparisons. To retrieve the top- k maximum values, this popping and maintenance process is repeated k times.

Note that after repeating the maintenance process multiple times, there may be cases where both leaf nodes under a certain non-leaf node are popped out. For instance, after retrieving the top-3 largest values, both child nodes of node 7 may be popped out. In this case, the MUX of node 7 outputs negative infinity for the register update on its parent node (node 3) in the subsequent cycle. Obviously, as long as the tree is not entirely emptied, i.e., fewer than N elements have been popped out, this negative infinity cannot propagate all the way to the root node.

Combining two trees into *Orizuru* A key advantage of *Orizuru*'s two-fold binary tree architecture is its ability to reuse the max tree's results to reduce the number of comparisons needed for the min tree. Given the limited number of comparators, the runtime bottleneck in *Orizuru* occurs during the initial tree setup, which requires $N/2$ comparisons. However, the comparison results from this step can be directly reused to initialize the min tree. Specifically, the registers at the $\log_2(N)$ -th level of the min tree can adopt the reversed comparison results from the max tree. This allows the min tree's initialization to skip the $\log_2(N)$ -th level and begin directly at the $(\log_2 N - 1)$ -th level, reducing the total comparisons for its initialization by 50%.

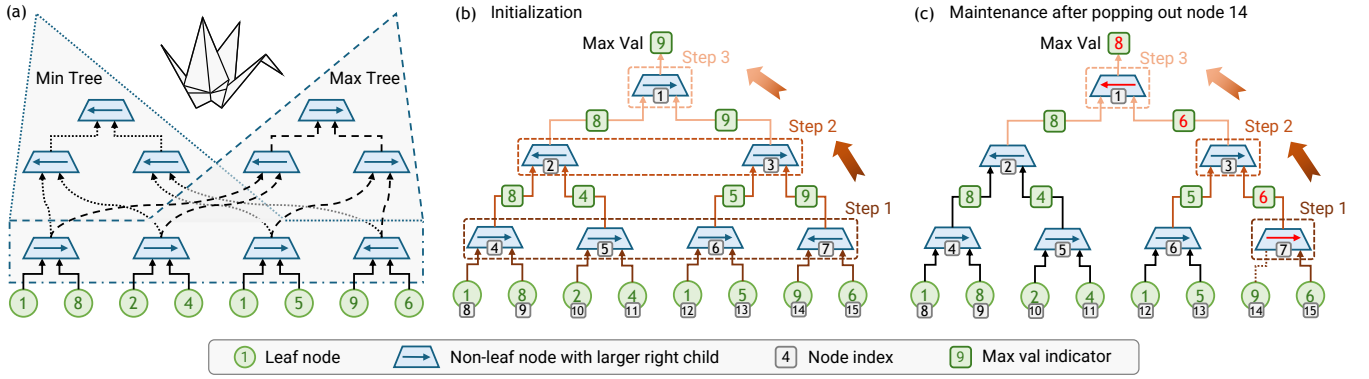


Fig. 7. Orizuru architecture. (a) The overall architecture of Orizuru: two-fold binary trees with shared leaf nodes and comparison results at the last layer of the non-leaf nodes. (b) Initialization of the max tree. (c) Maintenance of the max tree after popping out node 14.

V. EVALUATION

A. Experimental Setup

Models and Tasks We examine the algorithm performance of KLLM on a spectrum of LLMs and tasks. Specifically, the models include LLaMA-7B/13B/30B [47], LLaMA-2-7B/13B/70B [48], and Mistral-7B [24], which are implemented using the Transformers library [54] of Hugging Face [53] on top of the PyTorch [37] framework. These LLMs are evaluated on two tasks: (i) the next-word prediction task using the WikiText-2 dataset [34], measured by the PPL metric, and (ii) the zero-shot accuracy task across five common sense datasets: PIQA (PQ) [6], ARC-easy (ARC-e) [9], ARC-challenge (ARC-c) [9], HellaSwag (HS) [59], and WinoGrande (WG) [42]. The zero-shot performance evaluation utilizes the Language Model Evaluation Harness [15] framework, with zero-shot accuracy as the evaluation metric. All experiments are performed on a single NVIDIA A100-80GB GPU.

KLLM’s K-WAQ Implementation Details In KLLM, both weights and activations are quantized using K-Means clustering. Weights undergo 4-bit per-output-channel quantization without outlier protection, while activations are quantized per-token with 3/4-bit precision. The quantization centroids and indices for weights are precomputed offline, whereas the activation centroids are also trained offline using 16 calibration samples from the C4 dataset [11], and the indices are computed online during inference via K-Means clustering [33]. The offline centroids are trained using a weighted-K-Means algorithm, where the weights are determined by Fisher information matrices [38] of the activations. To handle outliers, the top 0.5% largest and bottom 0.5% smallest activation values are preserved in FP16 format, while the inliers are quantized. During inference, KLLM dynamically identifies outliers using the *Orizuru* units, while KLLM-S reuses the thresholds from the offline training process on the calibration dataset.

Baseline LLM Quantization Methods We compare KLLM with existing I-WAQ methods of round-to-nearest (RTN), SmoothQuant [55], QuaRot [3], and Atom [61]. Except for Atom, which uses group-wise quantization for both weights

and activations with a group size of 128, all other baseline algorithms employ per-output-channel quantization for weights and per-token quantization for activations. Baseline I-WAQ methods utilize the same W4A4 and W4A3 precision configurations as KLLM.

Architecture Modeling and Comparison The hardware performance of the KLLM architecture is modeled using a cycle-accurate simulator modified from DnnWeaver [43]. The area and power metrics of the core logic units in the KLLM accelerator, including the Concat unit, FP16 MAC unit, Index Distribution Counter, and *Orizuru*, are derived from synthesis results using the TSMC 28 nm standard cell library. Table I shows the detailed configurations of the hardware components on-chip. We use Cacti [29] and DRAMSim3 [28] to simulate the overhead of on-chip SRAM and off-chip HBM, respectively. We denote W4A3 KLLM as KLLM-A3 and W4A4 KLLM as KLLM-A4, and similarly for KLLM-S. We compare the hardware performance of KLLM with a series of baseline hardware accelerators, including the GPU-based platforms and ASIC accelerators. The GPU-based platforms include NVIDIA A100-80GB GPU [36], QuaRot [3], and Atom [61]. The ASIC accelerators include SpAtten [49], Olive [17], and BitMoD [8]. SpAtten reduces computational complexity in the attention mechanism through dynamic token and attention head pruning; MECLA employs aggressive weight compression using a scaling sub-matrix partitioning approach; Olive introduces an outlier-victim-pair quantization technique; and BitMoD designs customized FP data types tailored to the weight distributions in LLMs. The hardware performance of KLLM and the baseline accelerators are evaluated on the next-word-prediction task with an output sequence length of 2048.

B. Algorithm Performance Analysis

Table II shows the WikiText-2 PPL results for KLLM and baseline I-WAQ methods across various models with a sequence length of 2048. KLLM consistently achieves the lowest PPL for both W4A4 and W4A3 precisions, outperforming the I-WAQ methods. For LLaMA-2-7B at W4A4, KLLM achieves a PPL of 5.90, with only a 0.43 degradation from the

TABLE II
WIKITEXT-2 PPL WITH THE SEQUENCE LENGTH OF 2048.

Precision	Method	LLaMA-7B	LLaMA-13B	LLaMA-30B	LLaMA-2-7B	LLaMA-2-13B	LLaMA-2-70B	Mistral-7B
FP16	–	5.68	5.09	4.10	5.47	4.88	3.32	5.25
W4A4	RTN	8e3	1e4	3e5	2e3	7e3	2e5	6e3
	SmoothQuant	4e2	67.2	32.5	7e2	56.6	10.5	5e2
	QuaRot	6.34	5.58	4.64	6.19	5.45	3.83	5.77
	Atom	6.25	5.52	4.61	6.12	5.31	3.73	5.76
	KLLM-S	6.08	5.38	4.40	6.00	5.21	3.60	5.84
	KLLM	6.04	5.37	4.38	5.90	5.19	3.55	5.75
W4A3	RTN	2e4	2e4	1e4	6e5	5e5	6e5	1e4
	SmoothQuant	5e4	2e4	2e4	8e3	1e4	1e4	9e3
	QuaRot	29.75	19.02	13.50	2e2	2e2	85.28	2e2
	Atom	9.62	7.36	6.18	11.40	8.00	5.05	10.83
	KLLM-S	7.60	6.28	5.31	7.91	6.99	4.13	7.42
	KLLM	7.17	6.21	5.10	7.49	6.43	4.05	7.27

TABLE III
ZERO-SHOT ACCURACY OF LLaMA-2-7B.

Precision	Method	Zero-Shot Accuracy					
		PQ	ARC-e	ARC-c	HS	WG	Avg.
FP16	–	78.67	74.58	46.16	75.95	68.98	68.87
W4A4	QuaRot	76.77	69.87	40.87	72.16	63.77	64.69
	Atom	75.14	52.99	38.40	69.37	62.75	59.73
	KLLM-S	77.31	71.46	42.92	72.57	64.80	65.81
	KLLM	77.97	73.06	43.60	74.32	65.51	66.89
W4A3	QuaRot	72.17	60.26	35.37	63.61	60.48	58.38
	Atom	71.01	48.63	33.49	62.54	59.50	55.03
	KLLM-S	75.14	63.93	37.37	67.58	63.93	61.59
	KLLM	75.84	65.99	39.59	68.28	64.17	62.77

FP16 model, which is 34% lower than Atom’s degradation. Additionally, KLLM reduces PPL by 0.05 at W4A4 and 0.27 at W4A3 compared to KLLM-S, highlighting the benefits of dynamic outlier detection. Detailed comparisons of hardware efficiency between KLLM/KLLM-S are provided in §V-D.

We observe that for the LLaMA-2-7B and 13B models, W4A3 quantization methods of SmoothQuant, QuaRot, Atom, and KLLM demonstrate higher PPL compared to their counterparts in the LLaMA-7B and 13B models. This may be attributed to the 2nd generation of LLaMA models being *overtrained* on extensive training data, which makes post-training quantization challenging, particularly when the activation precision is low [26].

Table III shows the zero-shot accuracy results of KLLM on five common sense tasks. On average, KLLM introduces only a 1.98% and 6.1% accuracy drop at W4A4 and W4A3 precision levels, respectively, compared to the FP16 baseline, while significantly outperforming state-of-the-art I-WAQ methods. In the W4A4 setting, KLLM improves accuracy by 7.16% and 2.2% compared to Atom and QuaRot, respectively. Under the W4A3 configuration, KLLM achieves accuracy improvements of 7.74% over Atom and 4.39% over QuaRot.

C. Hardware Performance Analysis

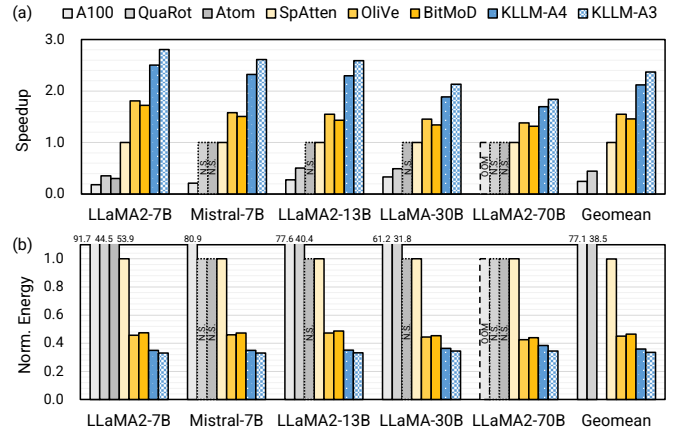


Fig. 8. Speedup and normalized energy consumption of KLLM and baseline accelerators in single-batch decoding.

Figure 8 shows the speedup and normalized energy consumption of KLLM and baseline accelerators in single-batch decoding. The baseline accelerators include GPU-based platforms: A100 (FP16), QuaRot (W4A4) and Atom (W4A4), and ASIC accelerators: SpAtten (FP8), Olive (W4A4), and BitMoD (W4A4). The speedup and energy consumption are normalized to that of SpAtten. N.S. indicates that the accelerator does not support the corresponding model, while OOM indicates that the accelerator runs out of memory for the specified model. Since LLaMA-2-7B is the only model that Atom supports, we don’t include the geometric mean of Atom in the figure. As shown in Figure 8(a), on average, KLLM-A4 achieves $8.66\times$, $4.76\times$, $2.12\times$, $1.37\times$, $1.45\times$ speedup and KLLM-A3 achieves $9.67\times$, $5.31\times$, $2.37\times$, $1.53\times$, $1.62\times$ speedup over A100, QuaRot, SpAtten, Olive, and BitMoD, respectively. For the A100 GPU, the operations during the single-batch decoding are generally memory-bound, which significantly limits its ability to deliver higher performance. QuaRot and Atom apply quantization on both weights and

activations. This not only enhances arithmetic intensity but also enables the use of integer compute units. However, their throughput is still limited by the low utilization of Tensor Cores at small batch sizes, which is an inherent limitation of GPU-based designs. With the optimizations discussed in §V-A, the baseline ASIC accelerators achieve higher speedup than the GPU-based platforms. However, compared to KLLM, the area efficiency of the compute units in the baseline ASIC accelerators is limited, which results in a constrained number of on-chip compute units and consequently demonstrates lower speedup. Figure 8(b) shows the normalized energy consumption of KLLM and baseline accelerators. Similar to the trends of speedups, on average, KLLM-A4 achieves $214.8\times$, $107.2\times$, $47.6\times$, $2.79\times$, $1.53\times$, $1.26\times$, $1.29\times$, and KLLM-A3 achieves $229.5\times$, $114.58\times$, $50.89\times$, $2.98\times$, $1.63\times$, $1.34\times$, $1.38\times$ energy efficiency improvement over A100, QuaRot, SpAtten, Olive, and BitMoD, respectively.

D. Ablation Studies

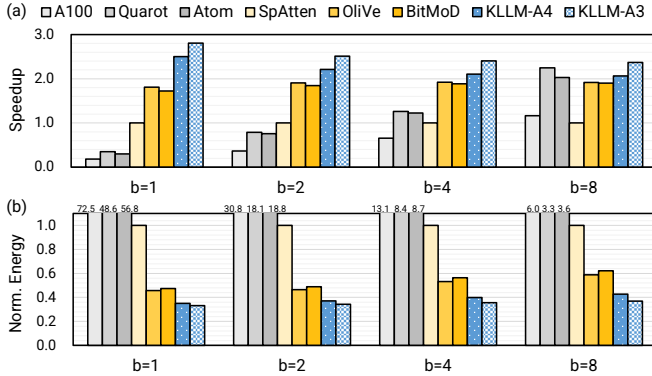


Fig. 9. Speedup and normalized energy consumption of KLLM and baseline accelerators during batched-decoding.

Batched-Decoding In Figure 9, we present the speedup and normalized energy consumption comparison of KLLM-A4/A3 over the baseline accelerators across different input batch sizes with the LLaMA-2-7B model. The speedup and energy consumption are normalized to that of SpAtten. As the batch size increases, all accelerators exhibit higher throughput and lower energy consumption, primarily due to increased arithmetic intensity from weight reuse. For the relative performance, GPU-based methods demonstrate a consistent throughput improvement as batch sizes grow, attributed to the higher utilization of Tensor Cores on GPUs with larger batch sizes [35]. Nonetheless, KLLM-A4 and KLLM-A3 still achieve $1.78\times$ and $2.04\times$ speedup over A100 at the batch size of 8.

Outlier Percentage Table IV presents the PPL results of KLLM with different outlier percentages, ranging from 0.5% to 10%. For each configuration of KLLM, increasing the outlier percentage improves the model’s PPL. We conclude that keeping 1% of the outliers in W4A4 KLLM is able to achieve a PPL increase of 0.43 over the FP16 baseline,

TABLE IV
WIKITEXT-2 PPL OF KLLM WITH DIFFERENT OUTLIER PERCENTAGES ON LLAMA-2-7B MODEL (FP16 BASELINE: 5.47).

Precision	Method	Outlier Percentage				
		0.5%	1%	2%	5%	10%
W4A4	KLLM-S	6.62	6.00	5.95	5.80	5.69
	KLLM	6.11	5.90	5.87	5.66	5.58
W4A3	KLLM-S	11.14	7.91	7.11	6.40	6.12
	KLLM	9.66	7.49	6.62	6.22	5.98

which is generally considered within an acceptable range of degradation. The impact of outlier percentage on throughput (tokens/s) with different versions of KLLM is shown in Figure 10(a). It is worthnoting that when keeping 1% of the outliers, KLLM only exhibits 6% - 8% lower throughput than KLLM-S under the same activation precision, which indicates the negligible overhead of the *Orizuru* units.

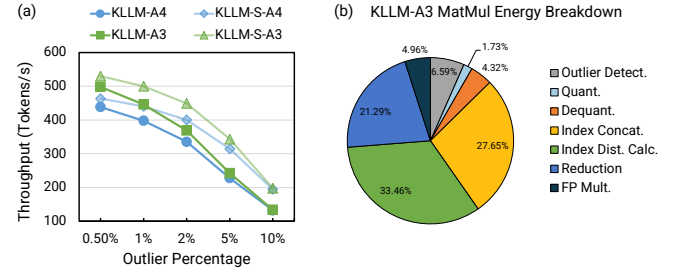


Fig. 10. (a) Throughput of KLLM across different outlier percentages. (b) On-chip energy breakdown for a MatMul between 4096×4096 weight and 1×4096 activation with KLLM-A3.

MatMul Energy Consumption Breakdown Figure 10(b) illustrates the on-chip energy consumption breakdown for each operation in a W4A3 MatMul between a 4096×4096 weight matrix and a 1×4096 activation vector with KLLM-A3. Here, “FP Mult.” refers to the energy consumed by sparse floating-point multiplications between activation outliers and weights, while “FP Add.” represents the energy used for floating-point additions that combine the partial results of sparse multiplications with dense multiplications. “Quant.” denotes the energy required for activation quantization, which is a single pass of clustering. “Dequant.” corresponds to the energy used for dequantization, which are lookup operations for the Cartesian products. The largest energy consumers are index concatenation, index distribution calculation, and reduction operations, accounting for 33.46%, 27.65%, and 21.02% of the total energy, respectively. Note that the dequantization process only contributes 4.32% of the total energy. This is because instead of dequantizing the entire weight and activation matrices, KLLM only dequantizes the Cartesian products of the indices, which are substantially smaller than the original matrices. The *Orizuru* units account for just 6.59% of the total energy, benefiting from energy-efficient design via the reuse of intermediate comparison results in the tree-based architecture.

Contributing Factors of PPL Improvement In Figure 11,

we analyze three factors contributing to the PPL from RTN to KLLM under the W4A3 precision: changing the integer quantization to the non-uniform K-Means quantization, which reduces the PPL from $>600,000$ to 8.03; adding sample weights to K-Means clustering based on the value sensitivity, which is discussed in §V-A, further reduces PPL to 7.91; and leveraging *Orizuru* for dynamic outlier detection, which reduces PPL to 7.49. Among these, non-uniform K-Means quantization is the most effective contributor to the PPL improvement.

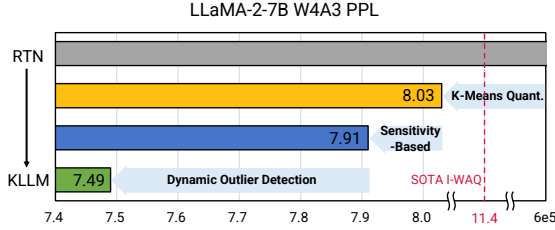


Fig. 11. PPL improvement breakdown of KLLM-A3.

Contributing Factors of Energy Efficiency Improvement Figure 12 demonstrates KLLM-A3’s energy efficiency improvements through the integration of each optimization technique. Baseline (A) represents an ASIC accelerator with FP16 compute unit arrays without any optimizations on memory or computation. (B) introduces weight quantization, reducing HBM energy by 75% and achieving a $2.49\times$ overall energy saving. Activation quantization in (C) enables the application of index-based MatMuls, further boosting the energy efficiency by $20.98\times$. Finally, (D) optimizes nonlinear operations in LLMs with the index-based computation scheme, resulting in an additional $1.45\times$ energy efficiency improvement.

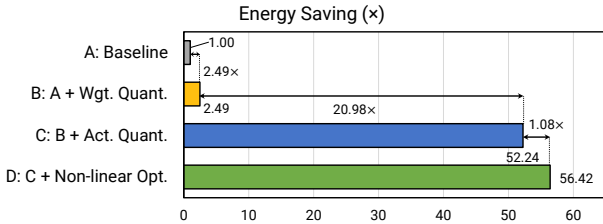


Fig. 12. Energy saving breakdown of KLLM-A3.

VI. RELATED WORKS

A. LLM Compression Techniques

LLM inference introduces significant costs for memory and computation due to the scale of model parameters [1], [12]. Besides quantization, a wide variety of model compression techniques have been proposed to mitigate these costs. Here, we discuss the two widely adopted techniques of pruning and singular value decomposition (SVD), and compare their effectiveness with quantization.

1) *Pruning*: Pruning has been adopted as an effective technique to compress LLM weights. Wanda [45] prunes weights with the smallest magnitudes multiplied by the corresponding input activations, which results in unstructured sparsity. LLM-Pruner [32] performs structured pruning on the weights by leveraging the Fisher information matrix for sensitivity detection. Pruning has also been applied to compress the KV Cache, and the resulting attention mechanism is referred to as sparse attention. THINK [57] removes insignificant channels, while FastGen [16] evicts long-range contexts and non-special tokens.

2) *SVD*: SVD compresses the models by approximating the original weight matrix with a low-rank representation [44]. SVD-LLM [52] and Dobi-SVD [50] identify the optimal truncation positions by a truncation-aware data whitening technique and a differentiable truncation mechanism, respectively.

Overall, pruning and SVD compress the LLMs by leveraging redundancy at the element level in weights and KV Cache. However, the compression ratios achievable with these methods are constrained to maintain model PPL, with maximum ratios of $2\times$ [45], $1.67\times$ [16], and $1.25\times$ [50], respectively. In contrast, quantization achieves compression by exploiting redundancy at the bit level within each element of weights and KV Cache, where LLMs exhibit greater redundancy compared to the element level. State-of-the-art WOQ methods achieve 4-bit quantization with minimal PPL degradation [25], [31], resulting in a $4\times$ compression ratio over FP16 models. Additionally, quantization facilitates the use of low-precision compute units, making it a widely adopted and effective approach for accelerating LLM inference.

B. Transformer/LLM Accelerators

Besides general-purpose accelerators such as GPUs and TPUs, there have been various ASIC accelerators proposed for efficient inference of LLMs and Transformers. Some approaches focus on reducing the computational complexity of the attention mechanism: A3 [19] applies algorithmic approximations to the attention mechanism, and also introduces a pipeline design that leverages customized datapaths, parallelism, and lower precision quantization to reduce computation costs; SpAtten [49] uses dynamic token and attention head pruning to skip computations for less significant tokens and heads; DOTA [40] detects sparse attention graphs to eliminate weak connections in the attention mechanism. Some approaches focus on reducing the memory footprint of LLMs: MECLA [39] decomposes large weight matrices into the smaller source and derived sub-matrices, and only fetches the source sub-matrices from the off-chip memory; [30] performs low-precision WAQ by applying channel sorting and channel selection for both weights and activations.

VII. CONCLUSION

In this work, we propose KLLM, a hardware-software co-design framework that enables fast LLM inference with K-Means-quantization. Specifically, we propose an efficient index-based computation scheme for K-Means-quantized data

that avoids most of the dequantization overhead and reduces the computational complexity. The proposed index-based computation scheme enables efficient execution of MatMuls and nonlinear operations in LLM inference with K-Means-quantized data. To achieve efficient online detection of the outliers in the activations, we propose the design of *Orizuru*, a lightweight outlier detection engine. KLLM achieves speedups of $8.66\times$, $2.12\times$ and energy efficiency improvements of $214.76\times$, $2.79\times$ over the A100 GPU and SpAtten, respectively.

REFERENCES

- [1] J. Achiam, S. Adler, S. Agarwal, L. Ahmad, I. Akkaya, F. L. Aleman, D. Almeida, J. Altenschmidt, S. Altman, S. Anadkat *et al.*, “Gpt-4 technical report,” *arXiv preprint arXiv:2303.08774*, 2023.
- [2] S. Ashkboos, I. Markov, E. Frantar, T. Zhong, X. Wang, J. Ren, T. Hoefer, and D. Alistarh, “Quik: Towards end-to-end 4-bit inference on generative large language models,” *arXiv preprint arXiv:2310.09259*, 2023.
- [3] S. Ashkboos, A. Mohtashami, M. L. Croci, B. Li, P. Cameron, M. Jaggi, D. Alistarh, T. Hoefer, and J. Hensman, “Quarot: Outlier-free 4-bit inference in rotated llms,” *arXiv preprint arXiv:2404.00456*, 2024.
- [4] J. L. Ba, “Layer normalization,” *arXiv preprint arXiv:1607.06450*, 2016.
- [5] I. Beltagy, M. E. Peters, and A. Cohan, “Longformer: The long-document transformer,” *arXiv preprint arXiv:2004.05150*, 2020.
- [6] Y. Bisk, R. Zellers, J. Gao, Y. Choi *et al.*, “Piqa: Reasoning about physical commonsense in natural language,” in *Proceedings of the AAAI conference on artificial intelligence*, vol. 34, no. 05, 2020, pp. 7432–7439.
- [7] T. Brown, B. Mann, N. Ryder, M. Subbiah, J. D. Kaplan, P. Dhariwal, A. Neelakantan, P. Shyam, G. Sastry, A. Askell *et al.*, “Language models are few-shot learners,” *Advances in neural information processing systems*, vol. 33, pp. 1877–1901, 2020.
- [8] Y. Chen, A. F. AbouElhamayed, X. Dai, Y. Wang, M. Andronic, G. A. Constantinides, and M. S. Abdelfattah, “Bitmod: Bit-serial mixture-of-datatype llm acceleration,” in *2025 IEEE International Symposium on High Performance Computer Architecture (HPCA)*. IEEE, 2025, pp. 1082–1097.
- [9] P. Clark, I. Cowhey, O. Etzioni, T. Khot, A. Sabharwal, C. Schoenick, and O. Tafford, “Think you have solved question answering? try arc, the ai2 reasoning challenge,” *arXiv preprint arXiv:1803.05457*, 2018.
- [10] T. Dao, D. Fu, S. Ermon, A. Rudra, and C. Ré, “Flashattention: Fast and memory-efficient exact attention with io-awareness,” *Advances in Neural Information Processing Systems*, vol. 35, pp. 16 344–16 359, 2022.
- [11] J. Dodge, M. Sap, A. Marasović, W. Agnew, G. Ilharco, D. Groeneveld, M. Mitchell, and M. Gardner, “Documenting large webtext corpora: A case study on the colossal clean crawled corpus,” *arXiv preprint arXiv:2104.08758*, 2021.
- [12] A. Dubey, A. Jauhri, A. Pandey, A. Kadian, A. Al-Dahle, A. Letman, A. Mathur, A. Schelten, A. Yang, A. Fan *et al.*, “The llama 3 herd of models,” *arXiv preprint arXiv:2407.21783*, 2024.
- [13] S. Elfving, E. Uchibe, and K. Doya, “Sigmoid-weighted linear units for neural network function approximation in reinforcement learning,” *Neural networks*, vol. 107, pp. 3–11, 2018.
- [14] Y. Fu, Y. Zhang, Z. Yu, S. Li, Z. Ye, C. Li, C. Wan, and Y. C. Lin, “Gpt4aigchip: Towards next-generation ai accelerator design automation via large language models,” in *2023 IEEE/ACM International Conference on Computer Aided Design (ICCAD)*. IEEE, 2023, pp. 1–9.
- [15] L. Gao, J. Tow, B. Abbasi, S. Biderman, S. Black, A. DiPofi, C. Foster, L. Golding, J. Hsu, A. Le Noac’h, H. Li, K. McDonnell, N. Muennighoff, C. Ociepa, J. Phang, L. Reynolds, H. Schölkopf, A. Skowron, L. Sutawika, E. Tang, A. Thite, B. Wang, K. Wang, and A. Zou, “The language model evaluation harness,” 07 2024. [Online]. Available: <https://zenodo.org/records/12608602>
- [16] S. Ge, Y. Zhang, L. Liu, M. Zhang, J. Han, and J. Gao, “Model tells you what to discard: Adaptive kv cache compression for llms,” *arXiv preprint arXiv:2310.01801*, 2023.
- [17] C. Guo, J. Tang, W. Hu, J. Leng, C. Zhang, F. Yang, Y. Liu, M. Guo, and Y. Zhu, “Olive: Accelerating large language models via hardware-friendly outlier-victim pair quantization,” in *Proceedings of the 50th Annual International Symposium on Computer Architecture*, 2023, pp. 1–15.
- [18] D. Guo, D. Yang, H. Zhang, J. Song, R. Zhang, R. Xu, Q. Zhu, S. Ma, P. Wang, X. Bi *et al.*, “Deepseek-r1: Incentivizing reasoning capability in llms via reinforcement learning,” *arXiv preprint arXiv:2501.12948*, 2025.
- [19] T. J. Ham, S. J. Jung, S. Kim, Y. H. Oh, Y. Park, Y. Song, J.-H. Park, S. Lee, K. Park, J. W. Lee *et al.*, “A³: Accelerating attention mechanisms in neural networks with approximation,” in *2020 IEEE International Symposium on High Performance Computer Architecture (HPCA)*. IEEE, 2020, pp. 328–341.
- [20] Z. He, H. Wu, X. Zhang, X. Yao, S. Zheng, H. Zheng, and B. Yu, “Chateda: A large language model powered autonomous agent for

- eda,” in *2023 ACM/IEEE 5th Workshop on Machine Learning for CAD (MLCAD)*. IEEE, 2023, pp. 1–6.
- [21] D. Hendrycks and K. Gimpel, “Gaussian error linear units (gelus),” *arXiv preprint arXiv:1606.08415*, 2016.
- [22] C. Hooper, S. Kim, H. Mohammadzadeh, M. W. Mahoney, Y. S. Shao, K. Keutzer, and A. Gholami, “Kvquant: Towards 10 million context length llm inference with kv cache quantization,” *arXiv preprint arXiv:2401.18079*, 2024.
- [23] X. Hu, Y. Chen, D. Yang, S. Zhou, Z. Yuan, J. Yu, and C. Xu, “I-llm: Efficient integer-only inference for fully-quantized low-bit large language models,” *arXiv preprint arXiv:2405.17849*, 2024.
- [24] A. Q. Jiang, A. Sablayrolles, A. Mensch, C. Bamford, D. S. Chaplot, D. d. l. Casas, F. Bressand, G. Lengyel, G. Lample, L. Saulnier *et al.*, “Mistral 7b,” *arXiv preprint arXiv:2310.06825*, 2023.
- [25] S. Kim, C. Hooper, A. Gholami, Z. Dong, X. Li, S. Shen, M. W. Mahoney, and K. Keutzer, “Squeezellm: Dense-and-sparse quantization,” *arXiv preprint arXiv:2306.07629*, 2023.
- [26] T. Kumar, Z. Ankner, B. F. Spector, B. Bordelon, N. Muennighoff, M. Paul, C. Pehlevan, C. Ré, and A. Raghunathan, “Scaling laws for precision,” *arXiv preprint arXiv:2411.04330*, 2024.
- [27] W. Kwon, Z. Li, S. Zhuang, Y. Sheng, L. Zheng, C. H. Yu, J. Gonzalez, H. Zhang, and I. Stoica, “Efficient memory management for large language model serving with pagedattention,” in *Proceedings of the 29th Symposium on Operating Systems Principles*, 2023, pp. 611–626.
- [28] S. Li, Z. Yang, D. Reddy, A. Srivastava, and B. Jacob, “Dramsim3: A cycle-accurate, thermal-capable dram simulator,” *IEEE Computer Architecture Letters*, vol. 19, no. 2, pp. 106–109, 2020.
- [29] S. Li, K. Chen, J. H. Ahn, J. B. Brockman, and N. P. Jouppi, “Cactip: Architecture-level modeling for sram-based structures with advanced leakage reduction techniques,” in *2011 IEEE/ACM International Conference on Computer-Aided Design (ICCAD)*. IEEE, 2011, pp. 694–701.
- [30] W. Li, A. Hu, N. Xu, and G. He, “Quantization and hardware architecture co-design for matrix-vector multiplications of large language models,” *IEEE Transactions on Circuits and Systems I: Regular Papers*, vol. 71, no. 6, pp. 2858–2871, 2024.
- [31] J. Lin, J. Tang, H. Tang, S. Yang, W.-M. Chen, W.-C. Wang, G. Xiao, X. Dang, C. Gan, and S. Han, “Awq: Activation-aware weight quantization for on-device llm compression and acceleration,” *Proceedings of Machine Learning and Systems*, vol. 6, pp. 87–100, 2024.
- [32] X. Ma, G. Fang, and X. Wang, “Llm-pruner: On the structural pruning of large language models,” *Advances in neural information processing systems*, vol. 36, pp. 21 702–21 720, 2023.
- [33] J. MacQueen, “Some methods for classification and analysis of multivariate observations,” in *Proceedings of 5-th Berkeley Symposium on Mathematical Statistics and Probability/University of California Press*, 1967.
- [34] S. Merity, C. Xiong, J. Bradbury, and R. Socher, “Pointer sentinel mixture models,” *arXiv preprint arXiv:1609.07843*, 2016.
- [35] NVIDIA, “Tensor core performance: The ultimate guide,” Tech. Rep., 2019.
- [36] —, “Nvidia a100 tensor core gpu architecture,” Tech. Rep., 2020.
- [37] A. Paszke, S. Gross, F. Massa, A. Lerer, J. Bradbury, G. Chanan, T. Killeen, Z. Lin, N. Gimelshein, L. Antiga *et al.*, “Pytorch: An imperative style, high-performance deep learning library,” *Advances in neural information processing systems*, vol. 32, 2019.
- [38] J. Pennington and P. Worah, “The spectrum of the fisher information matrix of a single-hidden-layer neural network,” *Advances in neural information processing systems*, vol. 31, 2018.
- [39] Y. Qin, Y. Wang, Z. Zhao, X. Yang, Y. Zhou, S. Wei, Y. Hu, and S. Yin, “Mecla: Memory-compute-efficient llm accelerator with scaling sub-matrix partition,” in *2024 ACM/IEEE 51st Annual International Symposium on Computer Architecture (ISCA)*. IEEE, 2024, pp. 1032–1047.
- [40] Z. Qu, L. Liu, F. Tu, Z. Chen, Y. Ding, and Y. Xie, “Dota: detect and omit weak attentions for scalable transformer acceleration,” in *Proceedings of the 27th ACM International Conference on Architectural Support for Programming Languages and Operating Systems*, 2022, pp. 14–26.
- [41] B. Roziere, J. Gehring, F. Gloeckle, S. Sootla, I. Gat, X. E. Tan, Y. Adi, J. Liu, R. Sauvestre, T. Remez *et al.*, “Code llama: Open foundation models for code,” *arXiv preprint arXiv:2308.12950*, 2023.
- [42] K. Sakaguchi, R. L. Bras, C. Bhagavatula, and Y. Choi, “Winogrande: An adversarial winograd schema challenge at scale,” *Communications of the ACM*, vol. 64, no. 9, pp. 99–106, 2021.
- [43] H. Sharma, J. Park, D. Mahajan, E. Amaro, J. K. Kim, C. Shao, A. Mishra, and H. Esmaeilzadeh, “From high-level deep neural models to fpgas,” in *2016 49th Annual IEEE/ACM International Symposium on Microarchitecture (MICRO)*. IEEE, 2016, pp. 1–12.
- [44] G. W. Stewart, “On the early history of the singular value decomposition,” *SIAM review*, vol. 35, no. 4, pp. 551–566, 1993.
- [45] M. Sun, Z. Liu, A. Bair, and J. Z. Kolter, “A simple and effective pruning approach for large language models,” *arXiv preprint arXiv:2306.11695*, 2023.
- [46] T. Tao, J. Li, B. Tan, H. Wang, W. Marshall, B. M. Kanakiya, J. Hestness, N. Vassilieva, Z. Shen, E. P. Xing *et al.*, “Crystal: Illuminating llm abilities on language and code,” *arXiv preprint arXiv:2411.04156*, 2024.
- [47] H. Touvron, T. Lavril, G. Izacard, X. Martinet, M.-A. Lachaux, T. Lacroix, B. Rozière, N. Goyal, E. Hambro, F. Azhar *et al.*, “Llama: Open and efficient foundation language models,” *arXiv preprint arXiv:2302.13971*, 2023.
- [48] H. Touvron, L. Martin, K. Stone, P. Albert, A. Almahairi, Y. Babaei, N. Bashlykov, S. Batra, P. Bhargava, S. Bhosale *et al.*, “Llama 2: Open foundation and fine-tuned chat models,” *arXiv preprint arXiv:2307.09288*, 2023.
- [49] H. Wang, Z. Zhang, and S. Han, “Spatten: Efficient sparse attention architecture with cascade token and head pruning,” in *2021 IEEE International Symposium on High-Performance Computer Architecture (HPCA)*. IEEE, 2021, pp. 97–110.
- [50] Q. Wang, J. Ke, M. Tomizuka, Y. Chen, K. Keutzer, and C. Xu, “Dobi-svd: Differentiable svd for llm compression and some new perspectives,” *arXiv preprint arXiv:2502.02723*, 2025.
- [51] W. Wang, S. Zhou, W. Sun, P. Sun, and Y. Liu, “Sole: Hardware-software co-design of softmax and layernorm for efficient transformer inference,” in *2023 IEEE/ACM International Conference on Computer Aided Design (ICCAD)*. IEEE, 2023, pp. 1–9.
- [52] X. Wang, Y. Zheng, Z. Wan, and M. Zhang, “Svd-llm: Truncation-aware singular value decomposition for large language model compression,” *arXiv preprint arXiv:2403.07378*, 2024.
- [53] T. Wolf, L. Debut, V. Sanh, J. Chaumond, C. Delangue, A. Moi, P. Cistac, T. Rault, R. Louf, M. Funtowicz *et al.*, “Huggingface’s transformers: State-of-the-art natural language processing,” *arXiv preprint arXiv:1910.03771*, 2019.
- [54] —, “Transformers: State-of-the-art natural language processing,” in *Proceedings of the 2020 conference on empirical methods in natural language processing: system demonstrations*, 2020, pp. 38–45.
- [55] G. Xiao, J. Lin, M. Seznec, H. Wu, J. Demouth, and S. Han, “Smoothquant: Accurate and efficient post-training quantization for large language models,” in *International Conference on Machine Learning*. PMLR, 2023, pp. 38 087–38 099.
- [56] G. Xiao, Y. Tian, B. Chen, S. Han, and M. Lewis, “Efficient streaming language models with attention sinks,” *arXiv preprint arXiv:2309.17453*, 2023.
- [57] Y. Xu, Z. Jie, H. Dong, L. Wang, X. Lu, A. Zhou, A. Saha, C. Xiong, and D. Sahoo, “Think: Thinner key cache by query-driven pruning,” *arXiv preprint arXiv:2407.21018*, 2024.
- [58] Z. Yuan, Y. Shang, Y. Zhou, Z. Dong, Z. Zhou, C. Xue, B. Wu, Z. Li, Q. Gu, Y. J. Lee *et al.*, “Llm inference unveiled: Survey and roofline model insights,” *arXiv preprint arXiv:2402.16363*, 2024.
- [59] R. Zellers, A. Holtzman, Y. Bisk, A. Farhadi, and Y. Choi, “Hel-laswag: Can a machine really finish your sentence?” *arXiv preprint arXiv:1905.07830*, 2019.
- [60] B. Zhang and R. Sennrich, “Root mean square layer normalization,” *Advances in Neural Information Processing Systems*, vol. 32, 2019.
- [61] Y. Zhao, C.-Y. Lin, K. Zhu, Z. Ye, L. Chen, S. Zheng, L. Ceze, A. Krishnamurthy, T. Chen, and B. Kasicki, “Atom: Low-bit quantization for efficient and accurate llm serving,” *Proceedings of Machine Learning and Systems*, vol. 6, pp. 196–209, 2024.